CLINICAL ORAL IMPLANTS RESEARCH

Goran I. Benic
Manuel Sancho-Puchades
Ronald E. Jung
Hans Deyhle
Christoph H.F. Hämmerle

In vitro assessment of artifacts induced by titanium dental implants in cone beam computed tomography

Authors' affiliations:
Goran I. Benic, Manuel Sancho-Puchades, Ronald E. Jung, Christoph H.F. Hämmerle, Clinic of Fixed and Removable Prosthodontics and Dental Material Science, Center of Dental Medicine, University of Zurich, Zurich, Switzerland
Hans Deyhle, Biomaterials Science Center, University of Basel, Basel, Switzerland

Corresponding author:
Dr *Goran I. Benic*
Clinic of Fixed and Removable Prosthodontics and Dental Material Science
Center of Dental Medicine
University of Zurich
Plattenstrasse 11
CH-8032 Zurich, Switzerland
Tel.: +41 44 634 32 52
Fax: +41 44 634 43 05
e-mail: goran.benic@zzm.uzh.ch

Key words: artifact, cone beam computed tomography, dental implant, *in vitro*, radiology, titanium

Abstract

Objective: The objective of this study was to evaluate the geometric pattern and the intensity of artifacts around titanium implants in cone beam computed tomography (CBCT) using an *in vitro* model.

Material and methods: Ten test models, each containing one 4.1-mm-diameter titanium implant, were cast from a human mandible using silicone impression material and dental stone. Each model contained an implant in one of the following single-tooth gaps: 37, 36, 34, 33, 31, 41, 43, 44, 46, and 47. For control purposes, three models without implants were produced. Each model was scanned five times using a CBCT scanner. Gray values (GV) were recorded at eight circumferential positions around the implants at 0.5 mm, 1 mm, and 2 mm from the implant surface (GV_{Test}). GV were measured in the corresponding volumes of interest (VOI) in the models without implants ($GV_{Control}$). Differences of gray values (ΔGV) between GV_{Test} and $GV_{Control}$ were calculated as percentages. To detect differences between GV_{Test} and $GV_{Control}$, the 95% confidence interval (CI) was computed for the values of ΔGV. Repeated measures ANOVA was used for the comparison of ΔGV at 0.5 mm, 1 mm, and 2 mm from the implant surface.

Results: Artifacts reflected by altered GV were always present in the proximity of titanium implants, regardless of the implant position. When comparing GV_{Test} and $GV_{Control}$, increased GV were found at the buccal and lingual aspects of the implant sites, whereas regions with reduced GV were located along the long axis of the mandibular body of the test models. A significant decrease in artifact intensity was found with increasing distance from the buccal implant surface ($\Delta GV_{0.5\ mm}$: 45 ± 10% [SD], $\Delta GV_{1\ mm}$: 28 ± 14% [SD], $\Delta GV_{2\ mm}$: 14 ± 7% [SD]) ($P < 0.001$).

Conclusion: Artifacts around titanium implants in CBCT images were distributed according to a geometrical pattern.

Radiographic imaging of bone is an important diagnostic tool in implant dentistry (Harris et al. 2012). Intraoral peri-apical radiography is commonly used for the follow-up examination of dental implants, aiming at assessing the marginal bone level and detecting signs of failing osseointegration (Albrektsson et al. 1986). However, due to its two-dimensional nature, the diagnostic value of intraoral radiography is limited by geometric distortions and anatomical superimpositions (Tyndall & Brooks 2000; Patel 2009; Patel et al. 2009). In addition, intraoral radiography does not allow assessing those parts of the alveolar process, which are directly in front or behind an oral implant with respect to the source of radiation. To date, there is very little scientific evidence on the long-term amount of bone remodeling and the efficacy of bone regeneration procedures at buccal and oral aspects of dental implants in humans (Chiapasco & Zaniboni 2009; Teughels et al. 2009). In the context of clinical research, there is, therefore, a need to develop an effective method for postoperative monitoring of buccal and oral bone at dental implants (Klinge & Flemmig 2009).

Due to its ability to provide cross-sectional images at lower radiation doses compared with conventional multislice computed tomography (MCT), cone beam computed tomography (CBCT) has broadened diagnostic possibilities in dentistry (Rustemeyer et al. 2004; Ludlow et al. 2006; Ludlow & Ivanovic 2008). Numerous studies found that CBCT provides accurate linear measurements of dentomaxillofacial structures (Lascala et al.

Date:
Accepted 8 September 2012

To cite this article:
Benic GI, Sancho-Puchades M, Jung RE, Deyhle H, Hämmerle CHF. *In vitro* assessment of artifacts induced by titanium dental implants in cone beam computed tomography. *Clin. Oral Impl. Res.* **24**, 2013, 378–383
doi: 10.1111/clr.12048

2004; Suomalainen et al. 2008; Lamichane et al. 2009; Fatemitabar & Nikgoo 2010; Al-Ekrish & Ekram 2011). However, similarly to MCT (Kalender et al. 1987; Zhao et al. 2000), CBCT is prone to the appearance of artifacts generated by dental implants (Draenert et al. 2007; Razavi et al. 2010; Schulze et al. 2010). It is, hence, questionable whether or not CBCT represents an adequate technique for the assessment of structures in the close proximity of dental implants.

It is highly desirable to fully understand the benefits and shortcomings of the CBCT image based evaluation of peri-implant tissues and the nature of artifacts induced by dental implants. Therefore, the aim of this study was to evaluate the geometric pattern and the intensity of artifacts around titanium implants in CBCT using an *in vitro* model.

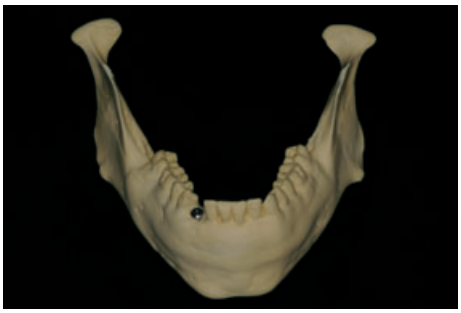

Fig. 1. Dental stone model containing a titanium implant in the single-tooth gap 43.

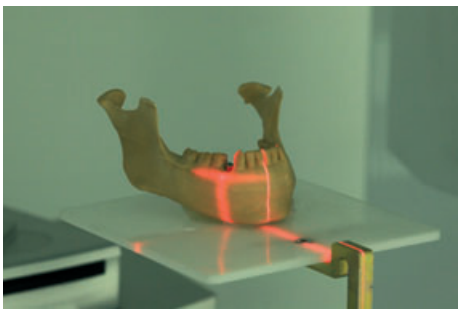

Fig. 2. Laser orientation beams used for the standardized positioning of the models in the CBCT scanner.

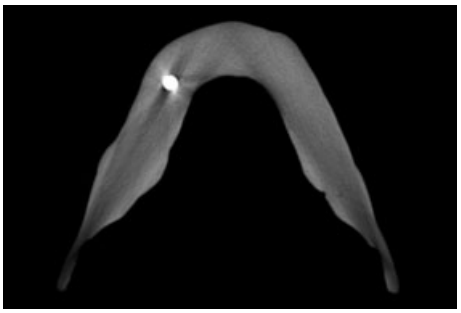

Fig. 3. Axial reconstruction perpendicular to the implant axis used for gray value measurements.

Material and methods

In vitro model

Ten test mandible models, each containing one 4.1 mm × 10 mm titanium implant (Straumann® Dental Implant System; Straumann AG, Basel, Switzerland), were cast using type IV dental stone (Noritake Super Rock; Noritake Co., Nagoya, Japan) (Fig. 1). Each model contained an implant in one of the following single-tooth gaps: 37, 36, 34, 33, 31, 41, 43, 44, 46, and 47.

A fully dentate dry human mandible was used for the production of the study models. Prior to the impression with silicone material (rema®-Sil; Dentaurum, Ispringen, Germany), a 1 mm thick layer of dental wax (Belladi Superior, Ruscher Belladi Dental Products, Altnau, Switzerland) was applied on the alveolar ridge to increase its dimension. Aiming at achieving a homogeneous dental stone density, the implants were positioned directly in the silicone mold, and each model was fabricated by a single plaster pour. Thereafter, 2-mm high titanium healing abutments (Straumann® Dental Implant System, Straumann AG, Basel, Switzerland) were placed on the implants.

For control purposes, three fully dentate models without implants were produced.

CBCT scanning

Each model was scanned five times using a 3D eXam CBCT device (KaVo Dental GmbH, Biberach, Germany), which is a version of i-CAT Next Generation scanner (Imaging Sciences International, Hatfield, PA, USA). For the scanning procedure, the models were mounted on the supporting plate provided by the manufacturer with the occlusal plane parallel to the horizontal plane and thereafter positioned in the center of field of view (FOV) using the laser orientation beams

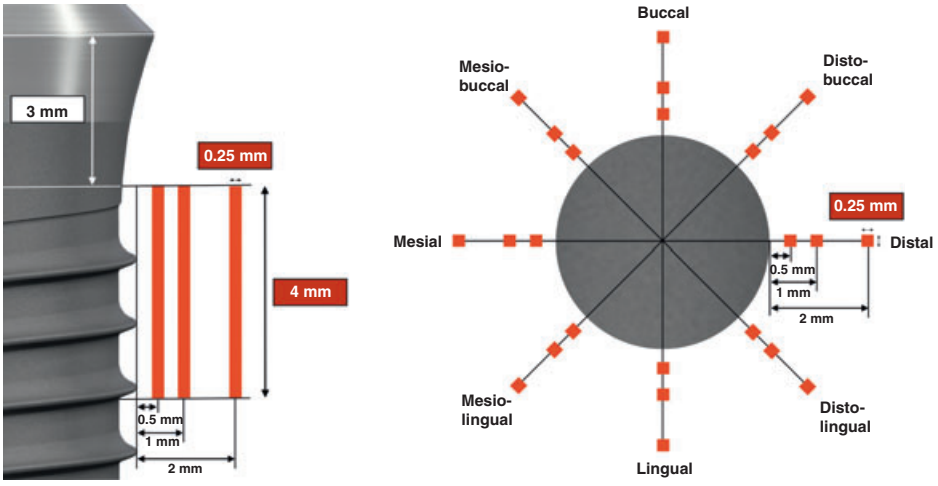

Fig. 4. Lateral and axial views of the volumes of interest (VOI) (in red) for gray value measurements.

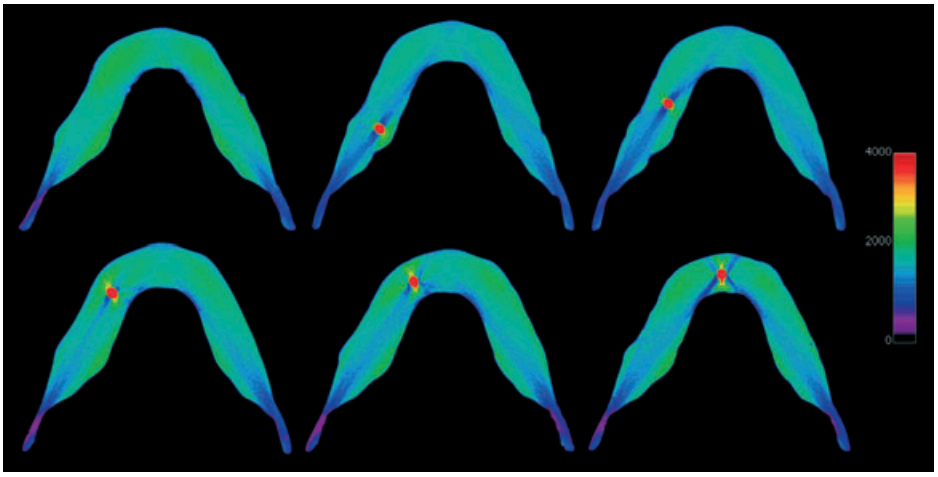

Fig. 5. Axial CBCT reconstructions of control and test models with the color-look-up-table (CLUT) of the gray values.

Table 1. **Mean differences of gray values between test and control models (ΔGV_{Mean}) for different circumferential positions and implant sites**

	Incisor			Canine			Premolar			First molar			Second molar		
	Mean ± SD	Range	95% CI	Mean ± SD	Range	95% CI	Mean ± SD	Range	95% CI	Mean ± SD	Range	95% CI	Mean ± SD	Range	95% CI
ΔGV_{Mean} (%)															
Buccal	40 ± 6	29 to 48	35; 45	22 ± 5	17 to 32	18; 26	28 ± 5	22 to 38	24; 32	27 ± 6	20 to 37	22; 32	28 ± 6	24 to 39	23; 33
Mesio-Buccal	−6 ± 11	−26 to 10	−16; 3	11 ± 16	−12 to 31	−2; 24	29 ± 5	21 to 35	24; 33	28 ± 5	20 to 34	25; 32	27 ± 8	15 to 38	21; 34
Mesial	5 ± 11	−10 to 20	−4; 13	−9 ± 7	−19 to 2	−15; −3	−32 ± 4	−39 to −25	−36; −28	−55 ± 8	−67 to −44	−61; −48	−50 ± 8	−61 to −37	−57; −43
Mesio-Lingual	−15 ± 7	−25 to −4	−21; −10	2 ± 8	−11 to 13	−5; 9	7 ± 14	−10 to 21	−5; 19	8 ± 15	−19 to 26	−4; 20	10 ± 9	−1 to 21	2; 17
Lingual	38 ± 13	11 to 52	27; 49	26 ± 15	9 to 54	13; 38	32 ± 3	27 to 36	29; 34	31 ± 8	16 to 38	25; 38	26 ± 5	20 to 34	22; 30
Disto-Lingual	−21 ± 6	−31 to −14	−26; −15	18 ± 7	7 to 25	12; 23	44 ± 5	34 to 50	39; 48	33 ± 8	23 to 47	26; 40	26 ± 5	21 to 34	22; 30
Distal	4 ± 4	−4 to 9	0; 7	−17 ± 15	−31 to 8	−30; −5	−40 ± 10	−52 to −28	−49; −32	−48 ± 13	−69 to −28	−59; −37	−46 ± 14	−65 to −22	−58; −34
Disto-Buccal	−6 ± 11	−19 to 12	−15; 4	5 ± 2	3 to 8	3; 7	17 ± 5	9 to 26	13; 21	10 ± 7	−2 to 20	4; 16	4 ± 11	−13 to 18	−6; 14

ΔGV_{Mean}, mean difference of gray values between test and control models; SD, standard deviation; CI, confidence interval.

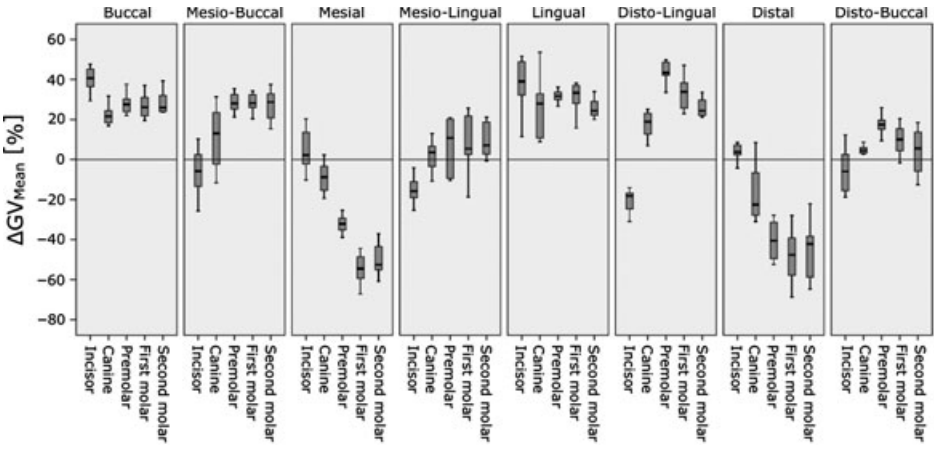

Fig. 6. Boxplots of mean differences of gray values between test and control models (ΔGV_{Mean}) for different circumferential positions and implant sites.

(Fig. 2). The scans were obtained with the following technical parameters: 120 kV acceleration voltage, 5 mA beam current, FOV diameter of 16 cm, FOV height of 6 cm, 600 projections, 360° rotation, voxel size of 0.25 mm, and scan time of 26 s.

CBCT image evaluation

CBCT 16-bit DICOM datasets were imported in the eXam Vision imaging software (KaVo Dental GmbH, Biberach, Germany). Axial reconstructions perpendicular to the implant long axis were used for the data evaluation (Fig. 3). The dimensions of the volumes of interest (VOI) were set to 0.25 mm × 0.25 mm in the axial plane and 4 mm in the implant long axis, resulting in a total VOI of 16 voxels (Fig. 4). Along the implant axis, VOI were set from 3 to 7 mm apically to the implant shoulder. X-ray attenuation expressed as gray value (GV) was recorded at eight different circumferential positions (buccal, mesio-buccal, mesial, mesio-lingual, lingual, disto-lingual, distal, and disto-buccal) at 0.5 mm, 1 mm, and 2 mm from the implant surface (Fig. 4). To facilitate the reproducibility of the assessment, a transparent acetate foil with printed implant and VOI outlines was placed on the computer monitor over the CBCT images. The software provided one mean GV for each VOI.

Subsequently, CBCT images of the control models without implants were evaluated. Anatomical landmarks on the model surface (e.g. teeth, alveolar ridge) were used to select volumes corresponding to those with implants in the test models. These volumes were marked by means of the previously described acetate foil with printed implant and VOI outlines. Thereafter, GV were measured in the VOI corresponding to those measured in the test models.

Data analysis

GV within VOI for the three control models without implants were averaged to $GV_{Control}$. Differences of gray values (ΔGV) between models with (GV_{Test}) and without ($GV_{Control}$) implants were calculated as percentages using the following formula: $\Delta GV = (GV_{Test} - GV_{Control})/GV_{Control} \times 100$.

ΔGV for the VOI at 0.5 mm ($\Delta GV_{0.5\ mm}$), 1 mm ($\Delta GV_{1\ mm}$), and 2 mm ($\Delta GV_{2\ mm}$) from the implant surface were averaged to ΔGV_{Mean}.

The data were visualized by means of box plots and described by mean values and standard deviations (SD) (PASW Statistics 18.0 software, IBM corporation, Somers, NY, USA). The assumption of normality of the data was tested using Kolmogorov–Smirnov and Shapiro–Wilk tests.

To detect the relevance of differences between GV_{Test} and $GV_{Control}$, the 95% confidence interval (CI) was computed for the values of ΔGV. If the value 0 was not contained within the 95% CI, there was statistical evidence that the mean value ΔGV was different from 0 at a significance level 0.05.

Repeated measures ANOVA together with Greenhouse-Geisser correction was used for the comparison of $\Delta GV_{0.5\ mm}$, $\Delta GV_{1\ mm}$, and $\Delta GV_{2\ mm}$. Results of tests with P-values $\leq$ 0.05 were considered statistically significant.

Results

Figure 5 presents CBCT images of the study models showing altered GV around titanium implants. To ease the readability of GV, a color conversion scala (UCLA color-look-up-table) was applied using OsiriX 3.7 imaging software (OsiriX Foundation, Geneva, Switzerland).

Table 2. Differences of gray values between test and control models for the volumes of interest at 0.5 mm ($\Delta GV_{0.5\ mm}$), 1 mm ($\Delta GV_{1\ mm}$), and 2 mm ($\Delta GV_{2\ mm}$) from the implant surface

	Incisor			Canine			Premolar			First molar			Second molar		
	Mean ± SD	Range	95% CI	Mean ± SD	Range	95% CI	Mean ± SD	Range	95% CI	Mean ± SD	Range	95% CI	Mean ± SD	Range	95% CI
	$\Delta GV_{0.5\ mm}$ (%)														
Buccal	45 ± 9	34 to 62	38; 53	35 ± 6	25 to 45	30; 40	45 ± 8	34 to 58	39; 52	47 ± 10	35 to 65	39; 55	52 ± 8	42 to 66	45; 59
Mesio-Buccal	6 ± 15	−20 to 28	−7; 18	11 ± 16	−14 to 34	−3; 24	31 ± 11	12 to 46	22; 40	35 ± 5	27 to 41	30; 39	34 ± 13	14 to 55	24; 45
Mesial	0 ± 18	−22 to 22	−15; 15	−11 ± 10	−27 to 3	−20; −2	−41 ± 9	−53 to −31	−48; −34	−67 ± 9	−81 to −51	−74; −59	−54 ± 12	−71 to −40	−64; −44
Mesio-Lingual	−12 ± 10	−33 to −4	−20; −4	7 ± 13	−14 to 25	−4; 17	2 ± 19	−20 to 24	−14; 18	−4 ± 20	−38 to 19	−20; 13	2 ± 12	−15 to 15	−8; 12
Lingual	52 ± 9	40 to 64	44; 59	44 ± 18	21 to 72	29; 58	58 ± 10	49 to 75	50; 67	50 ± 8	35 to 59	43; 57	35 ± 5	31 to 45	31; 39
Disto-Lingual	−8 ± 13	−25 to 11	−19; 3	22 ± 8	14 to 37	16; 28	52 ± 11	35 to 70	43; 62	42 ± 13	25 to 66	31; 53	33 ± 9	16 to 42	26; 40
Distal	−1 ± 10	−23 to 9	−10; 7	−25 ± 15	−40 to −1	−38; −13	−37 ± 11	−53 to −18	−47; −28	−49 ± 17	−76 to −23	−63; −35	−48 ± 16	−68 to −18	−62; −35
Disto-Buccal	2 ± 13	−12 to 24	−9; 13	9 ± 3	6 to 13	7; 11	19 ± 12	5 to 42	9; 28	0 ± 11	−20 to 14	−9; 9	−7 ± 21	−36 to 22	−24; 11
	$\Delta GV_{1\ mm}$ (%)														
Buccal	53 ± 6	45 to 63	48; 58	22 ± 2	18 to 24	20; 23	24 ± 5	19 to 35	20; 29	22 ± 9	8 to 38	14; 29	21 ± 7	14 to 35	15; 27
Mesio-Buccal	−6 ± 13	−26 to 11	−17; 5	11 ± 20	−17 to 36	−5; 28	32 ± 5	26 to 39	28; 36	30 ± 7	18 to 38	24; 35	29 ± 4	21 to 35	25; 33
Mesial	10 ± 10	−7 to 25	1; 18	−10 ± 8	−19 to −1	−16; −4	−35 ± 6	−42 to −25	−40; −30	−58 ± 7	−70 to −49	−64; −52	−54 ± 8	−63 to −38	−61; −47
Mesio-Lingual	−17 ± 6	−25 to −5	−22; −12	5 ± 5	−4 to 10	0; 9	8 ± 19	−17 to 25	−8; 24	12 ± 16	−19 to 29	−1; 25	11 ± 9	0 to 24	3; 19
Lingual	40 ± 23	−12 to 61	20; 60	21 ± 9	12 to 35	14; 29	25 ± 4	18 to 30	21; 28	28 ± 5	20 to 35	24; 32	22 ± 7	14 to 34	16; 28
Disto-Lingual	−23 ± 5	−31 to −18	−27; −19	15 ± 12	−5 to 27	4; 25	49 ± 6	38 to 58	43; 54	31 ± 17	−5 to 51	17; 45	28 ± 6	21 to 37	23; 33
Distal	8 ± 4	5 to 15	5; 11	−22 ± 15	−37 to 8	−35; −10	−45 ± 10	−58 to −32	−54; −37	−52 ± 15	−73 to −30	−64; −40	−47 ± 16	−67 to −22	−60; −33
Disto-Buccal	−5 ± 11	−19 to 10	−14; 4	4 ± 3	1 to 8	2; 6	21 ± 5	13 to 26	17; 25	14 ± 8	2 to 26	8; 21	8 ± 10	−6 to 23	−1; 17
	ΔGV_{2mm} (%)														
Buccal	23 ± 4	16 to 28	20; 27	9 ± 6	1 to 20	4; 14	13 ± 4	9 to 20	10; 17	12 ± 5	5 to 19	7; 16	12 ± 6	4 to 24	7; 17
Mesio-Buccal	−18 ± 8	−31 to −8	−25; −11	11 ± 13	−6 to 26	1; 22	23 ± 2	21 to 26	21; 25	21 ± 4	16 to 28	18; 24	18 ± 7	10 to 29	12; 24
Mesial	5 ± 6	−3 to 13	0; 9	−6 ± 14	−20 to 16	−18; 2	−21 ± 4	−26 to −15	−24; −17	−39 ± 8	−51 to −28	−46; −33	−42 ± 6	−49 to −31	−48; −39
Mesio-Lingual	−16 ± 9	−28 to −4	−23; −9	−6 ± 8	−15 to 5	−12; 1	10 ± 6	1 to 17	5; 14	16 ± 11	−3 to 31	7; 26	17 ± 7	4 to 26	11; 23
Lingual	22 ± 9	7 to 36	14; 30	12 ± 27	−12 to 62	−11; 35	8 ± 6	0 to 20	3; 13	16 ± 13	−9 to 31	5; 26	20 ± 4	15 to 28	16; 23
Disto-Lingual	−30 ± 6	−37 to −22	−35; −25	16 ± 14	−8 to 28	5; 28	30 ± 4	26 to 40	27; 34	26 ± 4	21 to 33	23; 30	17 ± 5	11 to 25	13; 21
Distal	5 ± 5	−2 to 13	0; 9	−4 ± 16	−23 to 20	−17; 10	−39 ± 10	−51 to −29	−47; −31	−44 ± 10	−58 to −31	−52; −35	−42 ± 11	−60 to −27	−52; −33
Disto-Buccal	−14 ± 10	−25 to 5	−22; −5	1 ± 5	−5 to 7	−2; 5	12 ± 3	9 to 17	10; 15	15 ± 7	2 to 24	9; 21	10 ± 10	−4 to 23	2; 19

$\Delta GV_{0.5\ mm}$, $\Delta GV_{1\ mm}$, and $\Delta GV_{2\ mm}$, difference of gray values between test and control models at 0.5 mm, 1 mm, and 2 mm from the implant surface; SD, standard deviation; CI, confidence interval.

The results of ΔGV_{Mean} for different circumferential positions and implant sites are presented in Table 1 and Figure 6. Table 2 contains the results of $\Delta GV_{0.5\ mm}$, $\Delta GV_{1\ mm}$, and $\Delta GV_{2\ mm}$.

ΔGV_{Mean} values differed considerably between different circumferential positions and implant sites, ranging from −55% to 44%. At the buccal and lingual aspects of all the sites, ΔGV_{Mean} showed positive values. In the samples with implants in the molar, premolar, and canine position, negative ΔGV_{Mean} were found mesially and distally. For the samples containing implants at incisor sites, negative ΔGV_{Mean} were generally found at the mesio-buccal, disto-buccal, disto-lingual, and mesio-lingual aspects (Table 1, Fig. 6).

When comparing measurements at different distances from the implant surface, considerable differences were found. At the buccal aspect, $\Delta GV_{0.5\ mm}$, $\Delta GV_{1\ mm}$, and $\Delta GV_{2\ mm}$ averaged for all the implant sites amounted at 45 ± 10% (SD), 28 ± 14% (SD), and 14 ± 7% (SD), respectively (Fig. 7). These values were significantly different from each other ($P < 0.001$).

Discussion

In the present *in vitro* CBCT study, artifacts reflected by altered gray values were always present in the proximity of titanium implants, regardless of the implant position. A pattern for the distribution of artifacts around titanium implants in CBCT was detected. In all specimens, increased gray values were found at the buccal and lingual aspects, whereas the regions with reduced gray values were located along the long axis of the mandibular body. In other words, regions with reduced gray values were located mesially and distally at the molar, premolar, and canine sites and at the mesio-buccal, disto-buccal, disto-lingual, and disto-buccal aspects of the incisor sites.

In a previous *in vitro* study, CBCT artifacts induced by titanium implants were investigated using a dental stone phantom of a mandibular premolar and molar region containing two implants and comparing two different CBCT scanners (Schulze et al. 2010). In the interproximal regions adjacent to the implants, a reduction of gray values of approximatively 50% was found. The degree of the gray value reduction decreased with increasing distance from the implant surface, which is in agreement with the results of the present study. Therefore, it was concluded that CBCT is unreliable for the evaluation of

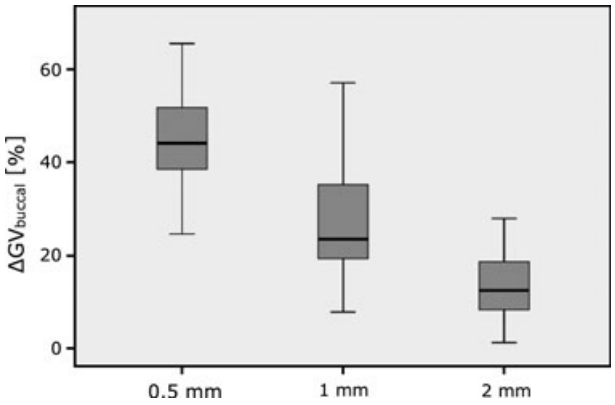

Fig. 7. Boxplots of differences of gray values between test and control models at the buccal aspect (ΔGV_{buccal}) for volumes of interest at 0.5 mm, 1 mm, and 2 mm from the implant surface.

the regions adjacent to the surface of metal implants. However, no data were provided with respect to the artifacts at the buccal and oral aspects of the implants.

In a recent *in vitro* study, the accuracy of two different CBCT scanners for measurements of cortical bone adjacent to implants was evaluated using bovine ribs (Razavi et al. 2010). The investigators found that the CBCT scanner with a spatial resolution of 0.125 mm provided accurate measurements in samples with a bone thickness > 0.8 mm. In a recent animal study, peri-implant bone defects were assessed by comparing the outcome of CBCT measurements to the histological standard (Corpas Ldos et al. 2011). Measurements on CBCT images underestimated the bone defect depth by approximately 1 mm compared with those from the histological slices. Nevertheless, there was a significant correlation between measurements on CBCT images and histological slices. In another *in vitro* study carried out on pig mandibles, the accuracy and quality of the representation of peri-implant defects by CBCT was investigated (Mengel et al. 2006). The study concluded that measurements from CBCT scans displayed only slight deviations in the extent of the peri-implant defects and that CBCT scans showed high imaging quality.

Thus, it can be assumed that despite its limitations in the presence of highly X-ray absorbing implants, CBCT has the potential for the quantitative assessment of buccal bone adjacent to implants and could provide valuable long-term data on biological processes that occur after implant placement and bone regeneration procedures.

A limitation of the present study was its *in vitro* set-up, which only partially simulated a clinical situation of CBCT scanning. It is known that the density response in CBCT depends on the total mass inside and outside the FOV (Bryant et al. 2008). In other words, the presence of anatomical structures (e.g. cranium, vertebral column) influences the gray value measurements of the jaw bones in CBCT. Differently from the jaw models used in this trial, the human jaws are heterogeneous structures made of various hard and soft tissues. In this study, the mandible models consisted of dental stone, because it is reasonable to assume that dense bone should have similar absorption properties due to the calcium component mainly determining X-ray absorption properties in both materials (Schulze et al. 2010).

It is important to be aware that in CBCT images, artifacts are always present in the close proximity of dental implants. However, no correlation between the artifact intensity and the inaccuracy of CBCT based dimensional measurements of peri-implant bone can be extrapolated from the findings of the present study.

The fact that gray value alterations in artifact-affected areas vary at different circumferential positions around an implant might have important implications, and its knowledge enables the clinician to better interpret CBCT images. For example, the identification of artifact-affected regions with reduced gray values could decrease the risk of false positive diagnosis of peri-implant bone defects.

At present, further investigations are needed to validate the CBCT for the evaluation of tissues around dental implants. Thanks to the rapid development in the field of 3D radiographic imaging, CT devices with improved accuracy, reduced radiation doses, and scan times can be expected in the coming years.

Finally, it is important to emphasize that in the absence of clinical symptoms or certain postoperative complications, there is no indication for follow-up imaging of dental implants by means of CBCT. Due to the higher radiation burden compared with the two-dimensional radiography, CBCT imaging cannot be justified where there is no direct benefit to the patient, except as part of ethically approved clinical research (Harris et al. 2012).

Conclusions

Within the limitations of the present *in vitro* study, it can be concluded that in CBCT images:

- Artifacts were always present in the proximity of titanium implants, regardless of the implant position.
- Compared to control models without implants, increased gray values were present at the buccal and lingual aspects of all the implant sites, whereas the regions with reduced gray values were located along the long axis of the mandibular body.
- A significant decrease in artifact intensity was found with increasing distance from the implant surface.

Acknowledgements: The investigators gratefully acknowledge the statistical assistance of Ph.D. Malgorzata Roos, Department of Biostatistics, University of Zurich, Switzerland. This study was supported by the Clinic of Fixed and Removable Prosthodontics and Dental Material Science, Center of Dental Medicine, University of Zurich, Switzerland. The implants were kindly provided by Straumann AG, Basel, Switzerland.

References

Albrektsson, T., Zarb, G., Worthington, P. & Eriksson, A.R. (1986). The long-term efficacy of currently used dental implants: a review and proposed criteria of success. *The International Journal of Oral & Maxillofacial Implants* **1**: 11–25.

Al-Ekrish, A.A. & Ekram, M. (2011). A comparative study of the accuracy and reliability of multidetector computed tomography and cone beam computed tomography in the assessment of dental implant site dimensions. *Dentomaxillofacial Radiology* **40**: 67–75.

Bryant, J.A., Drage, N.A. & Richmond, S. (2008) Study of the scan uniformity from an i-cat cone beam computed tomography dental imaging system. *Dentomaxillofacial Radiology* **37**: 365–374.

Chiapasco, M. & Zaniboni, M. (2009). Clinical outcomes of gbr procedures to correct peri-implant dehiscences and fenestrations: a systematic review. *Clinical Oral Implants Research* **20**(Suppl. 4): 113–123.

Corpas Ldos, S., Jacobs, R., Quirynen, M., Huang, Y., Naert, I. & Duyck, J. (2011). Peri-implant bone tissue assessment by comparing the outcome of intra-oral radiograph and cone beam computed tomography analyses to the histological standard. *Clinical Oral Implants Research* **22**: 492–499.

Draenert, F.G., Coppenrath, E., Herzog, P., Muller, S. & Mueller-Lisse, U.G. (2007). Beam hardening artefacts occur in dental implant scans with the newtom cone beam ct but not with the dental 4-row multidetector ct. *Dentomaxillofacial Radiology* **36**: 198–203.

Fatemitabar, S.A. & Nikgoo, A. (2010). Multichannel computed tomography versus cone-beam computed tomography: linear accuracy of in vitro measurements of the maxilla for implant placement. *The International Journal of Oral & Maxillofacial Implants* **25**: 499–505.

Harris, D., Horner, K, Grondahl, K., Jacobs, R., Helmrot, E., Benic, G.I., Bornstein, M.M., Dawood, A. & Quirynen, M. (2012). E.A.O. Guidelines for the use of diagnostic imaging in implant dentistry 2011. A consensus workshop organized by the European Association of Osseointegration at the Medical University of Warsaw. *Clinical Oral Implants Research* doi: 10.1111/j.1600-0501.2012.02441.x. [Epub ahead of print].

Kalender, W.A., Hebel, R. & Ebersberger, J. (1987). Reduction of ct artifacts caused by metallic implants. *Radiology* **164**: 576–577.

Klinge, B. & Flemmig, T.F. (2009). Tissue augmentation and esthetics (working group 3). *Clinical Oral Implants Research* **20**(Suppl. 4): 166–170.

Lamichane, M., Anderson, N.K., Rigali, P.H., Seldin, E.B. & Will, L.A.. (2009) Accuracy of reconstructed images from cone-beam computed tomography scans. *American Journal of Orthodontics and Dentofacial Orthopedics* **136**: 156 e151–e156; discussion 156–157.

Lascala, C.A., Panella, J. & Marques, M.M.. (2004) Analysis of the accuracy of linear measurements obtained by cone beam computed tomography (cbct-newtom). *Dentomaxillofacial Radiology* **33**: 291–294.

Ludlow, J.B., Davies-Ludlow, L.E., Brooks, S.L. & Howerton, W.B. (2006). Dosimetry of 3 cbct devices for oral and maxillofacial radiology: Cb mercuray, newtom 3g and i-cat. *Dentomaxillofacial Radiology* **35**: 219–226.

Ludlow, J.B. & Ivanovic, M. (2008). Comparative dosimetry of dental cbct devices and 64-slice ct for oral and maxillofacial radiology. *Oral Surgery, Oral Medicine, Oral Pathology, Oral Radiology, and Endodontology* **106**: 106–114.

Mengel, R., Kruse, B. & Flores-de-Jacoby, L. (2006). Digital volume tomography in the diagnosis of peri-implant defects: an in vitro study on native pig mandibles. *Journal of Periodontology* **77**: 1234–1241.

Patel, S. (2009). New dimensions in endodontic imaging: part 2. Cone beam computed tomography. *International Endodontic Journal* **42**: 463–475.

Patel, S., Dawood, A., Whaites, E. & Pitt Ford, T. (2009). New dimensions in endodontic imaging: part 1. Conventional and alternative radiographic systems. *International Endodontic Journal* **42**: 447–462.

Razavi, T., Palmer, R.M., Davies, J., Wilson, R. & Palmer, P.J. (2010). Accuracy of measuring the cortical bone thickness adjacent to dental implants using cone beam computed tomography. *Clinical Oral Implants Research* **21**: 718–725.

Rustemeyer, P., Streubuhr, U. & Suttmoeller, J. (2004). Low-dose dental computed tomography: significant dose reduction without loss of image quality. *Acta Radiologica* **45**: 847–853.

Schulze, R.K., Berndt, D. & d'Hoedt, B. (2010). On cone-beam computed tomography artifacts induced by titanium implants. *Clinical Oral Implants Research* **21**: 100–107.

Suomalainen, A., Vehmas, T., Kortesniemi, M., Robinson, S. & Peltola, J. (2008). Accuracy of linear measurements using dental cone beam and conventional multislice computed tomography. *Dentomaxillofacial Radiology* **37**: 10–17.

Teughels, W., Merheb, J. & Quirynen, M. (2009). Critical horizontal dimensions of interproximal and buccal bone around implants for optimal aesthetic outcomes: a systematic review. *Clinical Oral Implants Research* **20**(Suppl. 4): 134–145.

Tyndall, D.A. & Brooks, S.L. (2000). Selection criteria for dental implant site imaging: a position paper of the american academy of oral and maxillofacial radiology. *Oral Surgery, Oral Medicine, Oral Pathology, Oral Radiology, and Endodontology* **89**: 630–637.

Zhao, S., Robertson, D.D., Wang, G., Whiting, B. & Bae, K.T. (2000). X-ray ct metal artifact reduction using wavelets: an application for imaging total hip prostheses. *IEEE Transactions on Medical Imaging* **19**: 1238–1247.